

Conductance of the single-electron transistor: A comparison of experimental data with Monte Carlo calculations

C. Wallisser,^{*} B. Limbach,[†] P. vom Stein,[†] and R. Schäfer

Forschungszentrum Karlsruhe, Institut für Festkörperphysik, Postfach 3640, D-76121 Karlsruhe, Germany

C. Theis,[‡] G. Göppert, and H. Grabert

Fakultät für Physik, Albert-Ludwigs-Universität, Hermann-Herder-Straße 3, D-79104 Freiburg, Germany

(Dated: November 1, 2018)

We report on experimental results for the conductance of metallic single-electron transistors as a function of temperature, gate voltage and dimensionless conductance. In contrast to previous experiments our transistor layout allows for a direct measurement of the parallel conductance and no ad hoc assumptions on the symmetry of the transistors are necessary. Thus we can make a comparison between our data and theoretical predictions without any adjustable parameter. Even for rather weakly conducting transistors significant deviations from the perturbative results are noted. On the other hand, path integral Monte Carlo calculations show remarkable agreement with experiments for the whole range of temperatures and conductances.

PACS numbers: 73.23.Hk, 85.35.Gv, 02.70.Ss

I. INTRODUCTION

The usual single-electron transistor (SET) layout^{1,2} consists of two ultrasmall tunnel junctions with conductances $G_{s,d}$ and capacitances $C_{s,d}$, respectively. The junctions in series are biased by a voltage U_{sd} and the island between the tunneling barriers is coupled to a gate voltage U_g via a capacitance C_g .

This setup has been used as the basic device to study the Coulomb blockade³. Its transport properties are governed by two dimensionless parameters. Firstly, the dimensionless inverse temperature βE_c relates $\beta = (k_B T)^{-1}$ to the charging energy $E_c = e^2/(2C_\Sigma)$ with $C_\Sigma = C_s + C_d + C_g$ being the total island capacitance. This parameter determines how far the electrostatic blockade of the source-drain current is lifted by thermal excitations. Secondly, the dimensionless parallel conductance $g = (G_s + G_d)/G_K$, $G_K = e^2/h$ being the conductance quantum, measures how much the quantization of the island charge is smeared by quantum fluctuations. The charge on the island can be controlled by means of the gate voltage U_g . The linear-response conductance G between source and drain is a periodic function of U_g taking on values between G_{\min} and G_{\max} . Since the control of a device by Coulomb blockade exploits a large difference between G_{\min} and G_{\max} a detailed understanding of the washout of Coulomb blockade effects by thermal and quantum fluctuations is crucial for the optimal design of fast and reliable Coulomb blockade devices.

Theoretical work has mainly focused on the limits of small g or βE_c , respectively. In the weakly conducting regime, $g \ll 1$, perturbation theory^{4,5,6} should be sufficient to describe the experimental data. For $\beta E_c \ll 1$ it is more suitable to formulate the problem in terms of a path integral which may be evaluated semiclassically^{7,8,9}. Only recently the use of path integral Monte Carlo (PIMC) techniques was proposed to calculate the con-

ductance of the SET over the whole range of experimentally accessible parameters¹⁰. Especially the regime of large parallel conductance g is of interest for technological applications^{11,12,13}.

This recent work has pointed to a shortcoming of previous experiments. The first step of a comparison between theory and experiment is the determination of the parameters g and E_c . For the SET layout described above one can obtain only the series conductance G_Σ of the two junctions which does not suffice to calculate the dimensionless parallel conductance g without further assumption. Joyez et al.¹ assumed that their SETs were symmetric, i.e. built up of two identical tunnel barriers which turned out to be a good approximation for the first three samples measured in the experiment. However, comparing the data for the high conductance sample of Ref. 1 to their PIMC simulation results, Göppert et al.¹⁰ found strong indications that the tunnel barriers could be asymmetric.

Since an unambiguous determination of the relevant parameters is a prerequisite of a thorough comparison between theoretical and experimental results we have developed a transistor design with four tunnel junctions connected to the island (see Fig. 1). This arrangement allows the determination of the individual resistances of each junction and therefore the direct measurement of the tunneling strength parameter g . It is operated as SET by connecting two of the junctions in parallel to form source and drain, respectively.

In Sec. II we present experimental details about the sample fabrication, the determination of the parameters and the conductance measurements. In Sec. III we give the path integral formulation which is used for the imaginary time quantum Monte Carlo simulation. We summarize how the conductance can be calculated from the simulation data by use of the singular value decomposition (SVD) analytical continuation scheme. In Sec. IV we compare experimental and theoretical results. At low

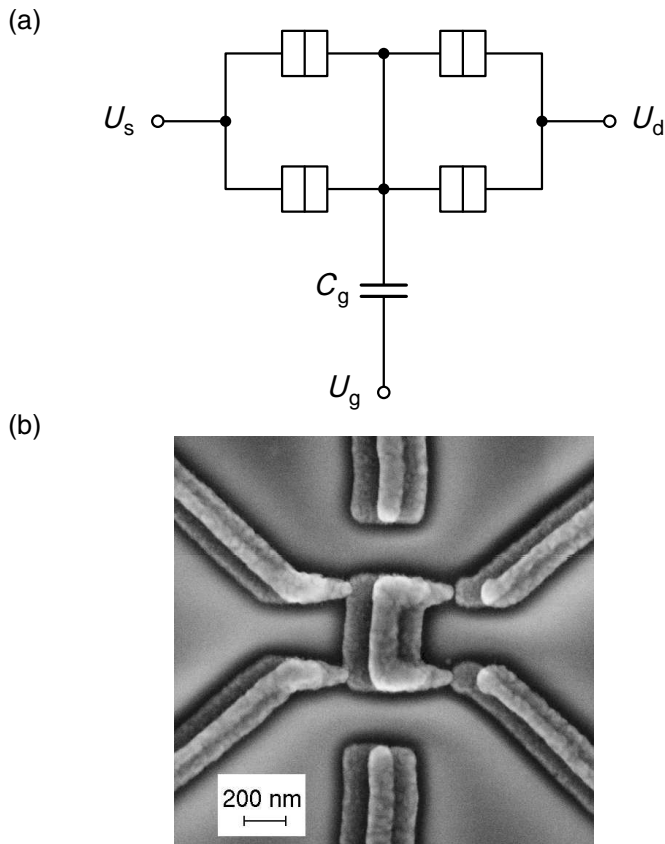


FIG. 1: a) Circuit diagram for the four junction layout when operated as SET. b) SEM picture of a four junction SET. The layout contains two symmetrically arranged gate fingers to avoid asymmetrical proximity effects in the lithography process. In the experiments both gates are connected in parallel.

conductance the perturbation theory is sufficient to describe the temperature dependence of G_{\max} , but for G_{\min} significant deviations are observed. At high conductance, we make a direct comparison of the experimental data with path integral Monte Carlo results.

II. EXPERIMENT

Seven samples with varying tunneling strengths were investigated. The samples were fabricated from aluminum by standard e-beam lithography in combination with two-angle shadow evaporation. The evaporation is performed by electrical heating a tungsten wire which holds a drop of aluminum. Tunnel barriers of different strengths could be produced by a variation of the oxygen pressure applied to the evaporation chamber between the two evaporation steps.

We used two different layouts: firstly, the usual SET design with two junctions, forming a small island in between, and a straight gate finger from the side pointing towards the island, secondly, the design which is shown

on the SEM picture in Fig. 1. In this design one can determine the individual tunnel resistances by measuring the current in response to an applied voltage bias across different combinations of the four tunnel junctions. The measurements presented in this article are performed on four standard SETs (samples I–IV), one four-contact sample (sample VII) and two samples which also have the four-contact layout, but turned out to have only three working tunnel junctions (samples V and VI). Nevertheless, this is sufficient to determine all individual tunnel resistances. The sample parameters are given in Table I. The measurements are performed in a top-loading dilution refrigerator in the temperature range from 25 mK to 18 K. The samples are mounted within a well-shielded metallic cavity. All electrical wiring into the cavity is made of highly resistive leads ($32 \Omega/\text{m}$, diameter 0.23 mm) which are fed through stainless steel capillaries with an inner diameter of 0.34 mm and a length of 1 m. The capillaries are wound up in a compact coil which is held in thermal equilibrium with the sample. These feedthroughs form resistive co-axial cables. They provide a damping exceeding 200 dB in the frequency range from 20 GHz to 6 THz, as calculated by classical electrodynamics taking the skin effect into account¹⁴. The validity of the used formulae was checked experimentally in the frequency range up to 20 GHz using a spectrum analyzer. Additional rf-filtering is performed at room temperature at the entrance to the cryostat.

To measure the conductance of the transistors they are biased with a voltage and the resulting current is measured with an operational amplifier at the top of the cryostat. The resolution of the current measurement is better than 100 fA. To gain resolution and to circumvent the $1/f$ -increase of noise at low frequencies an AC component of ≈ 10 Hz is added to the biasing DC voltage simultaneously and the resulting AC component of the current is measured with a lock-in amplifier. The DC measurement is used to ensure that the measurement is performed at vanishing bias and stays in the linear-response regime.

To determine the conductance G_{Σ} of two tunnel junctions in series, we measure the $I_{\text{sd}}U_{\text{sd}}$ characteristic up to a bias voltage of maximal ± 20 mV. We define the asymptotic slope at large bias voltages as G_{Σ} . The four-junction design allows six different configurations of two tunnel junctions connected in series. From the corresponding set $G_{\Sigma,i}$, $i = 1, \dots, 6$, the individual tunnel junction conductances can be derived with simple algebra. Their values are given in table I. Thus this layout enables us to actually measure the coupling strength parameter g directly. The SET investigated in the following experiments was formed by using all four tunnel junctions, where source and drain were made by connecting two tunnel junctions in parallel, respectively (see Fig. 1).

	G_{cl}^{-1} (k Ω)	C_{Σ} (aF)	C_g (aF)	G_s^{-1} (k Ω)	$G_{s'}^{-1}$ (k Ω)	G_d^{-1} (k Ω)	$G_{d'}^{-1}$ (k_B K)	E_c (k_B K)	g
I	128.0	220	25.6					4.25	0.80 (1.10)
II	74.7	240	27.6					3.87	1.39
III	19.2	250	27.5					3.70	5.38
IV	17.2	280	30.2					3.30	5.98
V	74.5	278	18.0	39.4		62.5	79.7	3.4	1.40
VI	59.4	344	18.0	22.7		104.2	56.1	2.7	1.85
VII	23.0	497	19.0	20.3	16.4	31.7	23.8	1.87	4.75

TABLE I: Parameters of the samples I–VII. G_{cl} denotes the high temperature conductance of the SET. The gate capacitance C_g is extracted from the period of the Coulomb oscillations within an accuracy of about 1%. Samples V–VII consist of at least three tunnel junctions. The individual conductances $G_{s,s'}$ and $G_{d,d'}$ for these samples were evaluated by simple algebra from values of G_{Σ} , which had been measured at different pairs of tunnel junctions as described in the text. For the 2-junction samples I–IV, the given value of g equals $(G_s + G_d)/(2G_K)$, an expression valid for symmetric SETs only. For the asymmetric sample I, the value derived from a comparison with the second-order perturbation theory is given in brackets (see Fig. 2).

III. THEORY

A. Path integral formulation

The linear DC conductance G represents a transport coefficient which can be expressed by correlation functions of the system using a Kubo formula¹⁰. Defining the current through the SET as the average of the current through the source and drain junctions $I = (I_s + I_d)/2$ the conductance G may be connected to the spectrum of the current autocorrelation function $F(t) = \langle I(t)I(0) \rangle$, i.e.

$$G = \frac{\beta}{2} \tilde{F}(\omega = 0) \quad (1)$$

with $\tilde{F}(\omega)$ denoting the Fourier transform of $F(t)$. The calculation of the current correlator may be done in the phase representation¹⁵, i.e. in terms of the phase variable φ which is conjugate to the charge q on the island. For imaginary time τ one gets⁸

$$F(\tau) = 4\pi G_{\text{cl}} \alpha(\tau) C(\tau) \quad (2)$$

with the classical high temperature conductance G_{cl} and

$$\alpha(\tau) = \frac{1}{2\pi} \int_{-\infty}^{\infty} d\omega \tilde{\alpha}(\omega) e^{-\tau\omega}, \quad (3a)$$

$$\tilde{\alpha}(\omega) = \frac{\hbar}{2\pi} \frac{\omega}{1 - e^{-\hbar\beta\omega}}. \quad (3b)$$

The cosine correlation function $C(\tau) = \langle \cos[\varphi(\tau) - \varphi(0)] \rangle$ has the formally exact path integral representation⁸

$$C(\tau) = \frac{1}{Z} \sum_{k=-\infty}^{\infty} \int_{\varphi(0)=0}^{\varphi(\beta\hbar)=2\pi k} \mathcal{D}\varphi e^{-\frac{1}{\hbar} S[\varphi] + 2\pi i k n_g} \times \cos[\varphi(\tau) - \varphi(0)] \quad (4)$$

with the partition function

$$Z = \sum_k \int \mathcal{D}\varphi e^{-\frac{1}{\hbar} S[\varphi]} e^{2\pi i k n_g} \quad (5)$$

and the dimensionless gate voltage $n_g = (U_g C_g)/e$. The Euclidian action $S[\varphi] = S_C[\varphi] + S_T[\varphi]$ splits into the Coulomb action

$$S_C[\varphi] = \int_0^{\beta\hbar} d\tau \frac{\hbar^2 \dot{\varphi}^2(\tau)}{4E_c} \quad (6)$$

which describes the charging of the island and the tunneling action

$$S_T[\varphi] = 2g \int_0^{\beta\hbar} d\tau \int_0^{\beta\hbar} d\tau' \alpha(\tau - \tau') \sin^2 \left[\frac{\varphi(\tau) - \varphi(\tau')}{2} \right] \quad (7)$$

that expresses the influence of tunneling processes on the dynamics of the phase variable φ .

Equation (4) may serve as the starting point for analytical calculations^{8,9} or numerical work¹⁰. In the latter case the interval $[0, \beta\hbar]$ is divided into N Trotter slices and the multidimensional integral is calculated using Monte Carlo methods^{16,17}. Since the action $S[\varphi]$ is real, the Metropolis algorithm can be applied for an importance sampling of the configurations $\{\varphi_i \equiv \varphi(\tau_i) | i = 0, \dots, N\}$ and the winding number k .

We did Monte Carlo simulations for fixed tunneling strength $g = 4.75$ over a range of inverse temperatures $\beta E_c \in [0.5, 21.0]$ which will be compared to our experimental findings in Section IV. For each temperature the system was equilibrated during several million Monte Carlo steps. Measurements were then carried out for another 5–32 million sweeps depending on the value of βE_c . Especially for low temperatures it is necessary to increase the number of measurements to get reliable statistics of the data. We ensured that the error of the correlation function is always less than 3%. Over the whole range

of temperatures we chose $N = 200$ Trotter slices fulfilling the convergence criterion $N \geq 5\beta E_c$ used in earlier work^{10,18}. The conductance was calculated for 200 values of the dimensionless gate voltage spanning the range $n_g \in [0, 0.5]$.

Additionally we examined single electron transistors with different parallel conductances $g \in [2.0, 15.0]$ for fixed temperature $1/(\beta E_c) = 0.05$. Here we chose $N = 250$ Trotter slices and did up to 23 million measurement sweeps. We found that the convergence was slower for small values of the dimensionless conductance.

B. Analytic continuation

Having calculated the cosine correlation function $C(\tau)$ using the PIMC method we still have to solve Eqs. (1) and (2) for the linear conductance G . With the positive and symmetric spectral function¹⁰ $A(\omega) = \tilde{C}(\omega)(1 - e^{-\beta\hbar\omega})/\omega$ one can write the Fourier transformation of $C(\tau)$ in imaginary time as

$$C = KA \quad (8)$$

where the integral operator K is given by

$$(KA)(\tau) = \frac{1}{2\pi} \int_0^\infty d\omega \frac{\omega \cosh\left[\left(\frac{\beta\hbar}{2} - \tau\right)\omega\right]}{\sinh\left(\frac{\beta\hbar}{2}\omega\right)} A(\omega) \quad (9)$$

and Eqs. (1) and (2) can be combined to give

$$G = \frac{\beta\hbar G_{cl}}{2\pi} \int_0^\infty d\omega \frac{\omega^2}{\cosh(\beta\hbar\omega) - 1} A(\omega). \quad (10)$$

Before we can calculate G using Eq. (10) it is necessary to invert the integral transform of Eq. (8) to obtain $A(\omega)$. This problem is similar to the analytical continuation of a function from the imaginary to the real axis¹⁹. It belongs to the class of *ill-posed* inverse problems. A straightforward inversion of Eq. (8) fails, because the integral operator K is almost singular and the statistical error in the data $C(\tau)$ is strongly amplified, making the result $A(\omega)$ meaningless. To deal with this problem, we use a recently developed method²⁰ based, upon the singular value decomposition of the integral operator.

From the SVD we get the singular system of K which fulfills

$$(Ku_j)(\omega) = \sigma_j v_j(\omega) \quad (11a)$$

$$(K^\dagger v_j)(\tau) = \sigma_j u_j(\tau) \quad (11b)$$

$$\sigma_0 \geq \sigma_1 \geq \sigma_2 \geq \dots \geq 0. \quad (11c)$$

The functions $u_j(\tau)$ and $v_j(\omega)$ are called the right and left singular vectors, respectively. The real and positive σ_j are the singular values of K . The formal solution to the inverse problem (8) is given as²⁰

$$A(\omega) = \sum_{j=0}^{\infty} \frac{c_j}{\sigma_j} v_j(\omega) \quad (12)$$

with the coefficients

$$c_j = \int_0^{\beta\hbar} d\tau C(\tau) u_j(\tau). \quad (13)$$

Since the numerical calculation of the correlation function $C(\tau)$ can only be done for a discrete set of points and additionally introduces a statistical error, the expansion coefficients (13) have a limited accuracy. Taking into account that for an ill-posed problem such as (8) the singular values σ_j vanish overexponentially with increasing j it becomes obvious that only the first few terms in the expansion (12) contain meaningful information whereas the higher terms will just corrupt the result by amplifying the noise of the data. This idea is used in the truncated SVD approach^{19,20} which truncates the summation in (12) by neglecting all terms for which σ_j/σ_0 is smaller than the statistical error of the correlation function $C(\tau)$.

Apart from Eq. (8) we still have supplementary information, namely that the spectral function $A(\omega)$ is positive and symmetric. To ensure positiveness one may use a "triangular window"²¹, i.e. in the truncated singular value decomposition one multiplies the singular values with a weight factor which falls off linearly from one to zero. Previous studies^{19,21} have shown that this implementation of positiveness reduces the resolution of the method. Recent work²⁰ has shown how to use supplementary information of positiveness to enhance the resolution of the singular value decomposition method. The idea is to determine additional expansion coefficients which cannot be inferred from the inverse problem. They can be fixed by the constraints that the result shall be positive and the difference to the truncated SVD solution shall be minimal. Further details about the implementation of the method can be found in Ref. 20.

The approach used in this work is limited only by the statistical error in the correlation function (4). The error of our PIMC calculation and the subsequent analytical continuation was estimated as follows. First we determined the statistical error of the Monte Carlo data. Then we produced an ensemble of data sets with different realizations of the error by adding Gaussian distributed random noise of the given size. The error bars shown in Figs. 4, 6 and 7 were then calculated from the maximum and minimum result of the analytical continuation.

IV. RESULTS AND DISCUSSION

In this section we present experimental data and theoretical results for the minimum and maximum linear response conductance, G_{\min} and G_{\max} , respectively, as a function of the dimensionless parallel conductance g and the temperature. Before we turn to the comparison between experimental and theoretical data we would like to summarize our findings about the determination of the experimental parameters.

The four-junction layout allows us to determine the dimensionless parallel conductance unambiguously offering

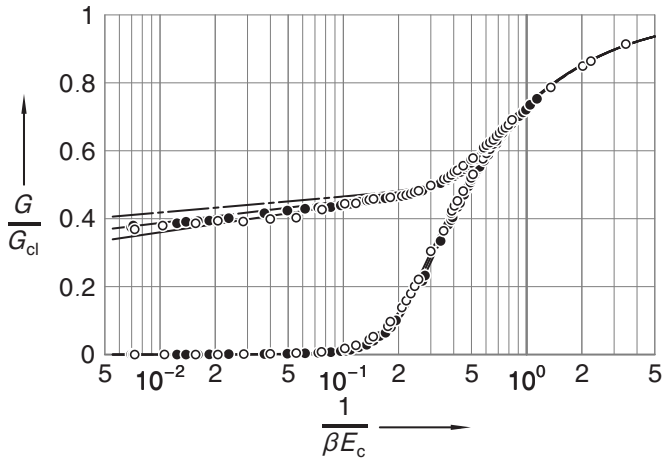


FIG. 2: G_{\max} and G_{\min} normalized to the high temperature conductance G_{cl} for sample I (●) and II (○) as a function of the normalized temperature. G_{\max} and G_{\min} are the maximum and minimum linear response conductance observed as a function of the gate voltage U_g , respectively. Lines correspond to the predictions of a second-order perturbative expansion in g (solid line: $g = 1.4$, dashed line: $g = 1.1$, dashed-dotted line: $g = 0.8$). The data are best described by $g = 1.1$ (●) and $g = 1.4$ (○).

the possibility of a direct comparison between experiment and theory. On the other hand measurements carried out on the two-junction samples I and II (see Fig. 2) clearly demonstrate a problem also encountered in Ref. 10. The assumption that the conductance is distributed equally among both tunnel junctions would lead to $g_{\text{I}} = 0.80$ and $g_{\text{II}} = 1.39$ for the samples I and II in contradiction to their almost identical temperature dependence of both G_{\min} and G_{\max} . Since the maximum conductance G_{\max} in the weak tunneling regime should fall off proportional to $g \ln(\beta E_c/\pi)$ for low temperatures⁵ Fig. 2 shows that the correct parallel conductances of those samples are almost equal. Our four-junction samples allow us to check this assumption directly (see below). We found that the tunnel junctions are *not identical* although they are produced simultaneously during shadow evaporation. This is not surprising as we tried to produce contacts with oxide barriers as thin as possible and very small junction areas. At the borderline between functioning and broken contacts the unavoidable variations in the fabrication procedure become visible as large fluctuations in the conductances of different junctions.

In previous experiments^{1,2,22} several methods for the determination of the charging energy E_c were proposed. As already mentioned in Ref. 2 the determination of the charging energy from the offset of the $I_{\text{sd}}U_{\text{sd}}$ curve is not very accurate. For sample V and VII we have analyzed the subgap resonances observed in the SET in the superconducting state to obtain the renormalized charging energy E_c^S as described in Ref. 1. Joyez et al. also give a perturbative result which connects E_c^S to the bare charging energy E_c ²⁵. Unfortunately it is only valid up

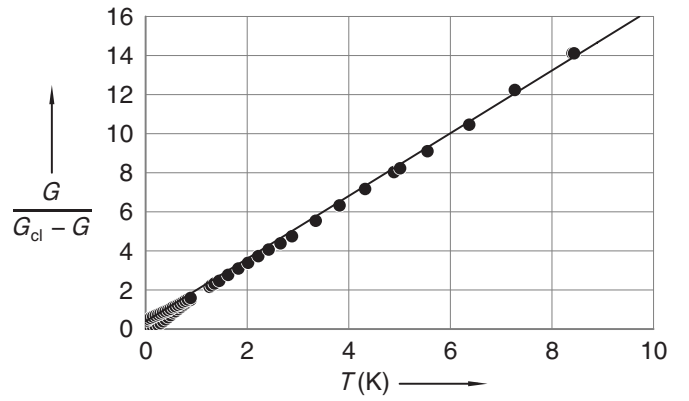


FIG. 3: Inverse conductance reduction $G/(G_{\text{cl}} - G)$ as a function of temperature. (●): Experimental data for sample VII, measured at vanishing source-drain voltage. (—): High-temperature expansion Eq. (14) with E_c chosen so as to fit the data.

to $\mathcal{O}(g^2)$. In our experiments we found that this is not sufficient for a description of high conductance single-electron transistors. In our opinion the best method for the determination of the charging energy is a comparison of the high-temperature experimental data to semiclassical calculations⁸. Apart from the full semiclassical expressions we tested the high-temperature expansion

$$\frac{G}{G_{\text{cl}} - G} = \frac{3k_B T}{E_c} + \frac{27g\zeta(3)}{2\pi^4} - \frac{2}{5} \quad (14)$$

using only data with $k_B T \gg g E_c / 2\pi^4$ (see Fig. 3). At a dimensionless conductance of $g = 4.75$ the difference in the charging energy between the full semiclassical result and Eq. (14) was less than 1%. In contrast to earlier work² sufficient experimental data at high temperatures are available for a determination of E_c . Moreover, Eq. (14) provides a consistency check for the dimensionless parallel conductance g which we have determined independently.

Having determined the experimental parameters we can turn to the comparison with the theoretical results. First of all we want to compare the data measured on sample I, III and V–VII with perturbation theory in second order in the parallel conductance g . Fig. 4 shows the maximum and minimum conductance of the single-electron transistor as a function of temperature. For sample I and V with their moderate $g = 1.1$ and $g = 1.40$, respectively, good agreement can be stated for G_{\max} . At higher g (sample III, VI and VII) deviations of increasing size are visible. Such deviations are not surprising as the perturbation expansion is not justified in this parameter range. For the minimum conductance G_{\min} we get deviations from the second-order result for all values of g investigated. At the lowest temperatures the determination of the minimum conductance G_{\min} is limited by the resolution of the lock-in signal which is of the order $10^{-3}G_0$. However the deviations are also prominent at $1/(\beta E_c) = 0.05$ where the lock-in signal has a sufficient

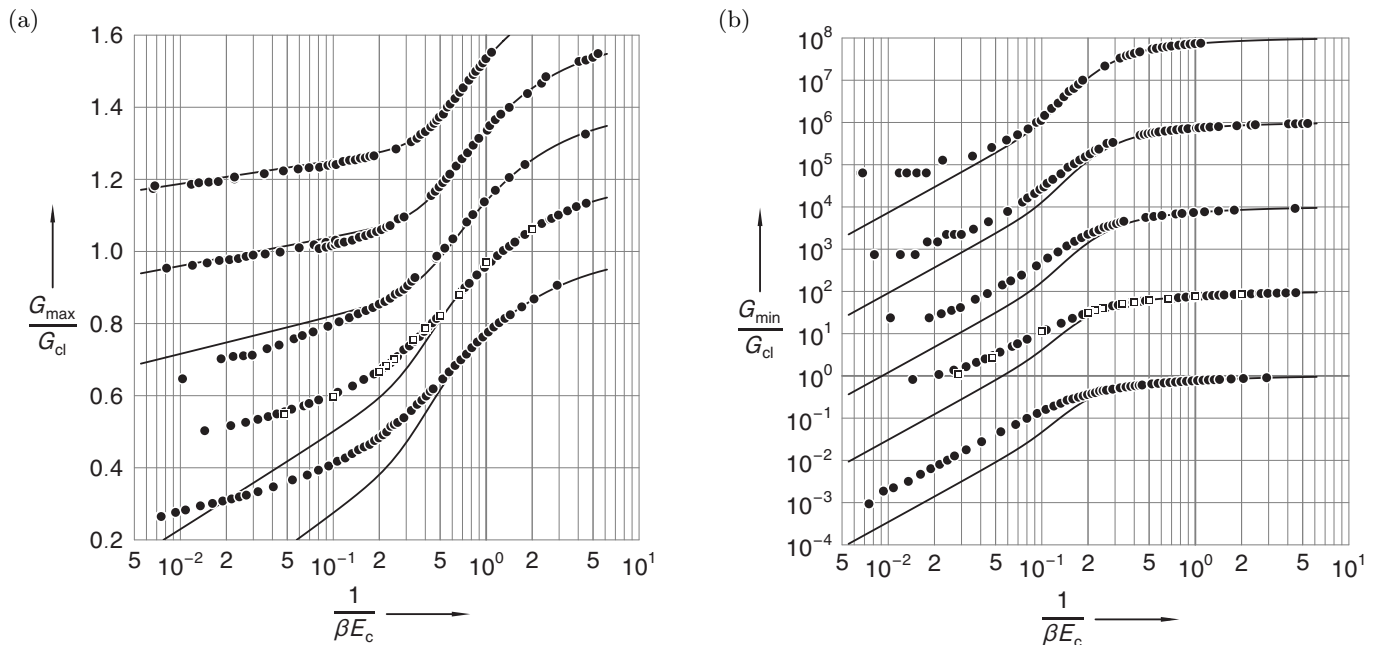


FIG. 4: Maximum (a) and minimum (b) conductance normalized to the high temperature conductance G_{cl} for samples I, V, VI, VII, and III with (from top to bottom) $g = 1.10, 1.40, 1.85, 4.75$, and 5.38 as a function of the normalized temperature. Together with the experimental data (\bullet) the predictions of the perturbation theory in second order ($—$) are shown for all samples. For sample VII the results of the Monte Carlo calculations (\square) are given additionally. For the sake of clarity the curves are plotted in (a) with a vertical offset increasing by 0.2 from curve to curve, in (b) the different datasets are multiplied by $10^2, 10^4$, etc.

accuracy. The discrepancy between perturbation theory and our data increases with g , indicating that higher-order corrections have to be included. With third-order perturbation theory²³ deviations for G_{min} are reduced but still visible.

Besides renormalization group methods²⁴ the quantum Monte Carlo approach is the only method which can cover the whole range of parameters that is accessible in the experiment. For sample VII ($g = 4.75$), which is beyond the perturbative regime, we perform a detailed comparison.

In Fig. 5 we show the gate voltage dependent conductance for inverse temperatures ranging from $1/(\beta E_c) = 0.048$ to $1/(\beta E_c) = 2.0$. We find that the experimental Coulomb oscillations are very well described by the Monte Carlo calculations. Minor discrepancies at some temperatures can be attributed to the fact that the temperatures used in the simulations do not exactly match those of the experimental data. For the lowest temperatures of the experiment it was not possible to get converged Monte Carlo results for the whole range of gate voltages in reasonable time.

In Fig. 6 the data are analyzed in terms of the minimum and maximum conductance. Once again the accordance is remarkable. For high βE_c the maximum conductance could not be determined by our Monte Carlo calculations. Here a limitation of the Monte Carlo procedure becomes obvious. For low temperatures more terms of the winding number summations in Eqs. (4) and (5) are

relevant leading to phase cancellations due to the factors $\exp(2\pi i k n_g)$ which are especially strong at $n_g = 0.5$, i. e. for the maximum conductance. Thus the convergence of the Monte Carlo procedure gets slower with decreasing temperature and the data cannot be determined as accurately. Since the analytic continuation is sensible to the statistical error of the data, reliable results for G_{max} could not be obtained with reasonable effort and the data points for G_{max} at the lowest temperatures have been omitted. This is not the case for the minimum conductance G_{min} as can be seen in the inset of Fig. 6. Here no phase cancellations occur and the experimental and theoretical data match nicely even on a logarithmic plot. We can also observe that in contrast to the perturbation theory in second order (cf. Fig. 4), the Monte Carlo approach gives an accurate description of G_{min} at low temperatures.

Finally we have examined the maximum and minimum conductance of single-electron transistors for varying tunneling strength g at a fixed temperature $1/(\beta E_c) = 0.05$. The results are shown in Fig. 7. Besides our experimental data the results of Joyez et al.¹ are shown. According to Ref. 10 the data of Joyez et al. at $g = 7.5$ has been displayed at $g = 10$. The Monte Carlo data include also the earlier results of Göppert et al.¹⁰. Once again we observe a reasonable accordance between theory and experiment. For $g > 8$ the comparison is hampered by uncertainties of the experimental parameters g and E_c . The parallel conductance of earlier experiments was system-

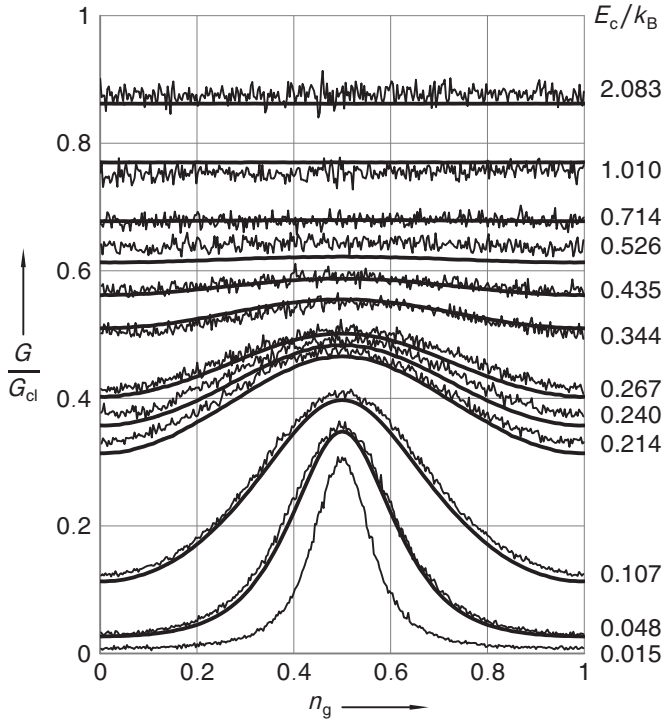


FIG. 5: Coulomb oscillations for sample VII ($g = 4.75$, thin lines) compared with Quantum Monte Carlo calculations (thick lines). The conductance G normalized to the high temperature conductance G_{cl} is shown as a function of the dimensionless gate voltage $n_g = (C_g U_g)/e$ for the temperatures as given in the right margin. The calculations were done at temperatures (from bottom to top) 0.048, 0.1, 0.2, 0.22, 0.25, 0.33, 0.4, 0.5, 0.67, 1.0 and 2.0 E_c/k_B .

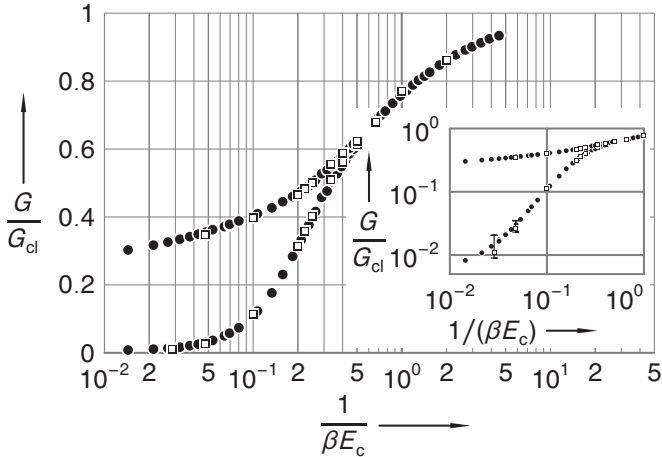


FIG. 6: Maximum and minimum linear response conductance G_{min} and G_{max} for sample VII ($g = 4.75$) normalized to the high temperature conductance G_{cl} . The experimental data (\bullet) are compared to the results of our PIMC simulation (\square). Data points for G_{max} at the lowest temperatures have been omitted (see text). The inset shows the same data on a logarithmic scale for better comparison of G_{min} . Errorbars are only shown if they exceed the symbol size.

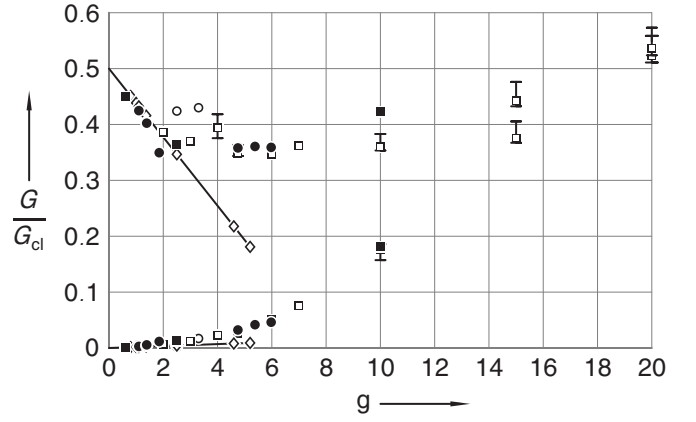


FIG. 7: Maximum and minimum conductance for $1/(\beta E_c) = 0.05$ as a function of the tunneling strength g for all examined samples (\bullet) in comparison with PIMC calculations (\square). Included are also the experimental data of Joyez et al.¹ (\blacksquare) and the results of perturbation theory in second order^{4,5} (\diamond) and third order²³ (\circ). Errorbars are only shown if they exceed the symbol size.

atically underestimated by the assumption of symmetry of the SET while for the determination of the charging energy E_c sufficient high temperature data were missing.

Also shown are the predictions of the perturbation expansion in second^{4,5} and third order²³ in g . The range of validity of the second-order perturbative approach is limited to $g \leq 2.5$ where the maximum conductance G_{max} drops with increasing g . The plateau and the following increase of the maximum conductance can not be described by perturbation theory. Also for G_{min} deviations occur at $g > 2.5$ while the Monte Carlo approach gives excellent results up to $g = 10$.

V. CONCLUSION

We have presented experimental results for the conductance of single-electron transistors as a function of temperature and dimensionless gate voltage. The employed four-junction layout for the SET allows for an unambiguous determination of the physical parameters g and E_c . Thus we were able to clarify and eliminate problems encountered in earlier experiments. In particular, comparison with theory can be made without any adjustable parameter. We have compared the experimental findings with perturbation theory in second order in g and with results of PIMC simulations.

Comparison with perturbation theory was made for the maximum and minimum conductance of five SETs with different tunneling strength. At $g < 1.85$ we found good agreement for the maximum linear conductance with second-order perturbation theory for the whole range of temperatures. Surprisingly even for such low-conductance SETs deviations from perturbation theory for G_{min} are pronounced at low temperatures. In con-

trast, a detailed comparison with PIMC data for $g = 4.75$ revealed good agreement between experiment and theory outside the perturbative regime. Further comparison showed that at $g = 4.75$ not only G_{\max} and G_{\min} but also the form of the Coulomb peaks could be described very well by our simulations for temperatures $1/(\beta E_c) \geq 0.05$.

Finally we have presented a comparison of experimental and theoretical results for the maximum and minimum conductance as a function of the tunneling strength g for a fixed temperature. The experimental data for this comparison are combined from experiments on different SETs including also the results of earlier experiments by Joyez et al.. For $g < 8$ we find that the PIMC data is in good accordance with experiment whereas perturbation theory in second order shows significant deviations for $g > 2.5$. Also the available data of third-order perturbation theory still show rather large deviations for G_{\max} .

The good agreement found in our study is an affirmation that the path integral formulation in combination with the Monte Carlo method allows for an accurate description of the minimum conductance G_{\min} over

the whole range of experimentally accessible parameters. Limitations of the Monte Carlo method for the calculation of the maximum conductance G_{\max} exist at low temperatures and small conductances due to slow convergence. Nonetheless G_{\max} as well as the entire shape of the Coulomb peaks can be described well in a range of parameters which lies outside the perturbative regime.

Acknowledgments

We would like to thank Bernhard Obst (Forschungszentrum Karlsruhe, Institut für Technische Physik) for supplying us with SEM images. We also thank B. Hüpfer, P. Joyez, J. König, H. Schoeller, A. I. Yanson, and H. v. Löhneysen for fruitful discussions. Financial support was provided by DFG through SFB 195 and SFB 276. C. W. and P. v. S. acknowledge financial support by the Landesgraduiertenförderung Baden-Württemberg.

-
- * Electronic address: Christoph.Wallisser@ifp.fzk.de; Also at Fakultät für Physik, Universität Karlsruhe, D-76128 Karlsruhe, Germany
- † Also at Fakultät für Physik, Universität Karlsruhe, D-76128 Karlsruhe, Germany
- ‡ Electronic address: theis@physik.uni-freiburg.de
- ¹ P. Joyez, V. Bouchiat, D. Esteve, C. Urbina, and M. Devoret, Phys. Rev. Lett. **79**, 1349 (1997).
 - ² D. Chouvaev, L. S. Kuzmin, D. S. Golubev, and A. D. Zaikin, Phys. Rev. B **59**, 10599 (1999).
 - ³ H. Grabert and M. H. Devoret, eds., *Single Charge Tunneling*, vol. 294 of *Nato Advanced Study Institute, Series B: Physics* (Plenum Press, New York, 1992).
 - ⁴ J. König, H. Schoeller, and G. Schön, Phys. Rev. Lett. **78**, 4482 (1997).
 - ⁵ J. König, H. Schoeller, and G. Schön, Phys. Rev. B **58**, 7882 (1998).
 - ⁶ H. Schoeller and G. Schön, Phys. Rev. B **50**, 18436 (1994).
 - ⁷ D. S. Glubev and A. D. Zaikin, JETP Lett. **63**, 1007 (1996).
 - ⁸ G. Göppert and H. Grabert, Phys. Rev. B **58**, R10155 (1998).
 - ⁹ G. Göppert and H. Grabert, Eur. Phys. J. B **16**, 687 (2000).
 - ¹⁰ G. Göppert, B. Hüpfer, and H. Grabert, Phys. Rev. B **62**, 9955 (2000).
 - ¹¹ P. Lafarge, H. Pothier, E. R. Williams, D. Esteve, C. Urbina, and M. H. Devoret, Z. Phys. B **85**, 327 (1991).

- ¹² A. N. Cleland, D. Esteve, C. Urbina, and M. H. Devoret, Appl. Phys. Lett. **61**, 2820 (1992).
- ¹³ J. P. Pekola, K. P. Hirvi, J. P. Kauppinen, and M. A. Paalanen, Phys. Rev. Lett. **73**, 2903 (1994).
- ¹⁴ A. B. Zorin, Rev. Sci. Instrum. **66**, 4296 (1995).
- ¹⁵ G. Schön and A. Zaikin, Phys. Rep. **198**, 237 (1990).
- ¹⁶ K. Binder and D. W. Heermann, *Monte Carlo Simulations in Statistical Physics* (Springer, Berlin, 1998).
- ¹⁷ M. Suzuki, ed., *Quantum Monte Carlo Methods in Condensed Matter Physics* (World Scientific, Singapore, 1993).
- ¹⁸ C. P. Herrero, G. Schön, and A. D. Zaikin, Phys. Rev. B **59**, 5728 (1999).
- ¹⁹ E. Gallicchio, S. A. Egorov, and B. J. Berne, J. Chem. Phys. **109**, 7745 (1998).
- ²⁰ G. D. de Villiers, B. McNally, and E. R. Pike, Inverse Problems **15**, 615 (1999).
- ²¹ M. Bertero, P. Brianzi, E. R. Pike, and L. Rebolia, Proc. R. Soc. London, Ser. A **415**, 288 (1988).
- ²² J. G. Lu, J. M. Hergenrother, and M. Tinkham, Phys. Rev. B **57**, 4591 (1998).
- ²³ H. Schoeller, J. König, F. Kuczera, and G. Schön, Journal of Low Temperature Physics **118**, 409 (2000).
- ²⁴ J. König and H. Schoeller, Phys. Rev. Lett. **81**, 3511 (1998).
- ²⁵ The formula given in Ref. 1 contains a typo. Instead of x/π the prefactor in the definition of $f(x)$ should read x/π^2 .